Scripta Materialia 207 (2022) 114310

Contents lists available at ScienceDirect

Scripta Materialia

journal homepage: www.elsevier.com/locate/scriptamat

Mechanical response of the constrained nanostructured layer in heterogeneous laminate

Yanfei Wang[a], Yueguang Wei[a,*], Zhifu Zhao[a], Zhongya Lin[a], Fengjiao Guo[b], Qian Cheng[b], Chongxiang Huang[b,*], Yuntian Zhu[c]

[a] Department of Mechanics and Engineering Science, College of Engineering, Peking University, Beijing 100871, China
[b] School of Aeronautics and Astronautics, Sichuan University, Chengdu 610065, China
[c] Department of Materials Science and Engineering, City University of Hong Kong, Hong Kong, China

ARTICLE INFO

Article history:
Received 15 July 2021
Revised 2 September 2021
Accepted 21 September 2021
Available online 1 October 2021

Keywords:
Heterostructure
Nanostructure
Strength and uniform elongation
Strain bands
Mechanical constraint

ABSTRACT

Understanding the inter-zone interaction-dependent mechanical behavior of constituent zones in heterostructured material is fundamental but challenging. Here we report quantitative investigations on the mechanical response of a nanostructured Cu-10Zn layer constrained by coarse-grained Cu layers in a laminate. The nanostructure layer displays large uniform elongation, moderate work hardening but gradually reduced engineering stress. Such unique responses are primarily attributed to the inter-layer constraint, which leads to the formation of dispersed stable strain bands and thus enables extensive activation of mechanical twinning and stacking faults. These findings provide new insights into the deformation and load-bearing mechanisms of heterostructures.

Metals and alloys designed with bionic heterogeneous microstructure, specifically consisting of zones with dramatically different mechanical properties, have recently attracted extensive research interests [1–3]. Combining the mechanical superiority of multiple types of zones, such as the high strength of nanostructure (NS) zone and the good ductility of coarse-grained (CG) zone, is the primary intention of this design route [4,5]. Optimized mechanical properties in strength-ductility combination and fracture resistance were indeed achieved in many heterostructured materials [4–11]. This makes heterostructure design an effective route in overcoming strength-ductility trade-off dilemma [1].

The deformation of heterostructures, however, cannot be simply evaluated basing on the performance of freestanding constituent zones, due to the heterostructural effect caused by strain incompatibility-rendered inter-zone interaction [4,9,12–14]. For examples, the incompatibility in elastic limit between neighboring zones introduces elastic/plastic interaction at the yielding stage, and the work hardening discrepancy causes plastically stable/unstable constraint at the large-strain stage. Such interactions change the internal stress and strain into triaxial gradient status, and enable dynamic inter-zone stress/strain transfer and partitioning [9,12–15]. As a result, extraordinary defect behaviors including unusual dislocation accumulation and annihilation may be activated [6,7,10]. Conjugate with these unique micromechanics, synergistic effects, i.e., extra responses in both strength and uniform elongation, were frequently reported in heterostructures [6–8,16–18]. A reasoning arising therefrom is that the behavior of a constituent zone may have been modified by inter-zone interactions [19]. This raises further question: how does the constituent zone behave during the deformation of a heterostructure? This question is fundamental for understanding the deformation mechanisms and optimizing heterostructure design.

At the yielding stage, geometrically necessary dislocations have to be accumulated near the interface of softer zones to accommodate the plastic strain gradient, which in turn produces back stress to strengthen the softer zones and forward stress to “weaken” the harder neighboring zones [20–22]. These physics shed qualitative light on the effects of elastic/plastic interaction. However, it is challenging to quantify the effects of such long-range internal stresses on zone behaviors. Soon after yielding, the plastic stability of NS zone depends largely on the synergistic constraint from ductile neighbor [7,13]. In both gradient structures and bimodal-grained material, dispersed strain bands were recently examined at this stage [23,24]. The strain bands evolved stably and played role in strain accommodation. But their effects on the strain hardening and flow strength of constituent zones, especially for the NS zone, remain unclear. Moreover, there is great curiosity about the universality of this mechanism. Measuring the lattice strain by in-situ synchrotron diffraction may enable a derivation of the strength-

* Corresponding authors.
E-mail addresses: weiyg@pku.edu.cn (Y. Wei), chxhuang@scu.edu.cn (C. Huang).

https://doi.org/10.1016/j.scriptamat.2021.114310
1359-6462/

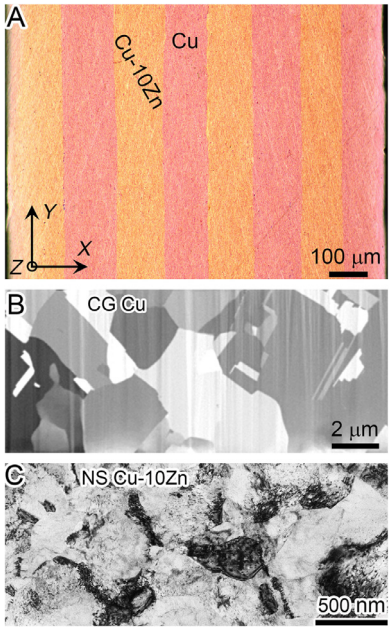

Fig. 1. Microstructure of laminate: (*A*) an optical image showing the stacking of Cu and Cu-10Zn layers, (*B*) ICCM image of the Cu layer, (*C*) TEM image of the Cu-10Zn layer. In the coordinate, *Y* is the rolling as well as the tensile loading direction, and *X* is the layer thickness direction.

strain response of designated zone [9,12], but such study in heterostructure is lacking.

Here we report a quantitative study on the behavior of constituent zone in heterostructure. Since the NS/CG laminate has the simplest architecture of heterogeneous zones, it is selected as a model sample. During the tensile deformation of laminate, stress-strain response of the NS layer is evaluated. It is surprisingly found that, under the constraint of CG neighbor, the NS layer displays unique and excellent performances in both strength and uniform elongation.

Laminates consisting of alternatively stacked pure copper and brass (Cu-10%wt.Zn) layers were fabricated by accumulative roll bonding (Fig. 1*A*) [8]. There is well-defined layer boundary with an average layer thickness of ~125 μm. After annealing at 220 °C for 2 h, microstructure of layers was examined using ion channeling contrast microscopy (ICCM) and transmission electron microscopy (TEM). As shown in Fig. 1*B*, the copper layer is characterized by recrystallized homogeneous CG with an average grain size of 4.8 μm. In contrast, severely deformed NS with high-density dislocations maintains in the brass layer due to the higher thermal stability (Fig. 1*C*). Such dramatic microstructure heterogeneity is expected to enable strong inter-layer constraint during straining [7,9,13].

A prestraning-peeling-retesting procedure was designed to characterize the stress-strain response of NS layer in laminate. Integrated laminate specimens were machined in dog-bone shape with a gauge dimension of $10 \times 2 \times 1\ mm^3$. After *x*% tensile prestrain, the NS layer of integrated laminate specimen was peeled off by polishing away other layers, and labeled as $NS_{x\%}$ specimen for another tensile test. $NS_{0\%}$ represents the freestanding NS layer undergone 0% prestrain. During the peeling process, the thickness of $NS_{x\%}$ specimens was elaborately controlled by referring to layer interface, and the thickness fluctuation along gauge length was controlled within 3 μm. All uniaxial tensile tests were carried out at a nominal strain rate of $5 \times 10^{-4}\ s^{-1}$. To ensure data reproducibility, tests of each type of $NS_{x\%}$ sample were repeated on at least 4 specimens.

Fig. 2*A* shows the engineering stress-strain curves. The colored solid curves represent the prestraining processes. The integrated laminate specimen displays an acceptable combination of yield strength (~280 MPa) and uniform elongation (~15%). In addition to the high strength of NS layer and the high strain hardening efficiency of CG layer, the hetero-deformation induced development of long-range internal stress was also reported to play critical roles in both the strengthening and work hardening [10,16,21,22]. The excellent uniform elongation of laminate may suggest that the NS layer in it was elongated coherently with CG layer to a decent strain [5,25].

Fig. 2*B* presents the true stress-strain curves. The yield strength, flow stress at 0.5% plastic strain and ultimate strength of $NS_{x\%}$ specimens were extracted and fitted as a function of the corresponding total true strain (including the prestrain), as the blue curve shown in Fig. 2*C*.

During prestraining in an integrated laminate, the strain incompatibility-rendered inter-layer interactions changed the stress state of NS layer, thereby affecting the multiplication and accumulation of defects [6,7,26]. Following that made in the theoretical deduction of hetero-deformation induced stress from hysteresis loop [21,27], it is assumed that, before unloading the prestrained laminate and after reloading the freestanding $NS_{x\%}$ specimen to yield, the relative change of microstructure in the NS layer is negligible. In other words, it is assumed that the yield strength of $NS_{x\%}$ specimen is largely determined by the unique microstructure formed during prestraining, and it represents the flow strength of constrained NS layer when the integrated laminate is deformed to *x*% strain. The fitted flow curve (Fig. 2*C*), therefore, can be approximately considered as the stress-strain response of NS layer in the tensile deformation of laminate.

Comparing the stress-strain curves reveals that mechanical behavior of the constrained NS layer in laminate (Fig. 2*C*) is dramatically different from that of its freestanding counterpart (the dotted red curve in Fig. 2*B*), i.e., the $NS_{0\%}$ specimen. First, the high flow strength of the constrained NS layer is accompanied by moderate work hardening. There is an increase in true flow strength, from a yield strength of ~515 MPa to ~562 MPa at 13.5% strain, although it is not strong. This is consistent with the slight hardness increment (the insert in Fig. 2*D*). In sharp contrast, a freestanding NS layer has no chance to achieve stable work hardening under tensile load [28].

Second, the constrained NS layer indeed displays excellent uniform elongation (Fig. 2*C*). As estimated from the flow stress increment, the average strain hardening rate at plastic strain stage (~350 MPa) is lower than the flow strength (>515 MPa). This indicates that, the critical strain, from which the work hardening is weaker than the geometrical softening, i.e.,

$$d\sigma_t A_t < -\sigma_t dA_t \tag{1}$$

should be much lower than 13.5%. $d\sigma_t$ and dA_t are the increment of true flow strength and the real-time cross-section shrinking, respectively. If this situation is met by a freestanding NS layer, fatal necking will be readily triggered by a local mechanical perturbation [29]. However, for the NS layer bonded to stable CG layer in a laminate, there is no free space to accommodate serious strain localization [30,31], and constraint from the latter can effectively arrest the unstable development of primary strain concentration, as discussed later in Fig. 4. This enables the NS layer to continue to elongate with homogeneous cross-section shrinking. In other words, uniform elongation of the constrained NS layer in laminate depends on both the work hardening and the inter-layer constraint. It is for this reason that the conventional Considère criterion, based on which the limit of uniform elongation is only determined by the work hardening rate, is invalid for it [29].

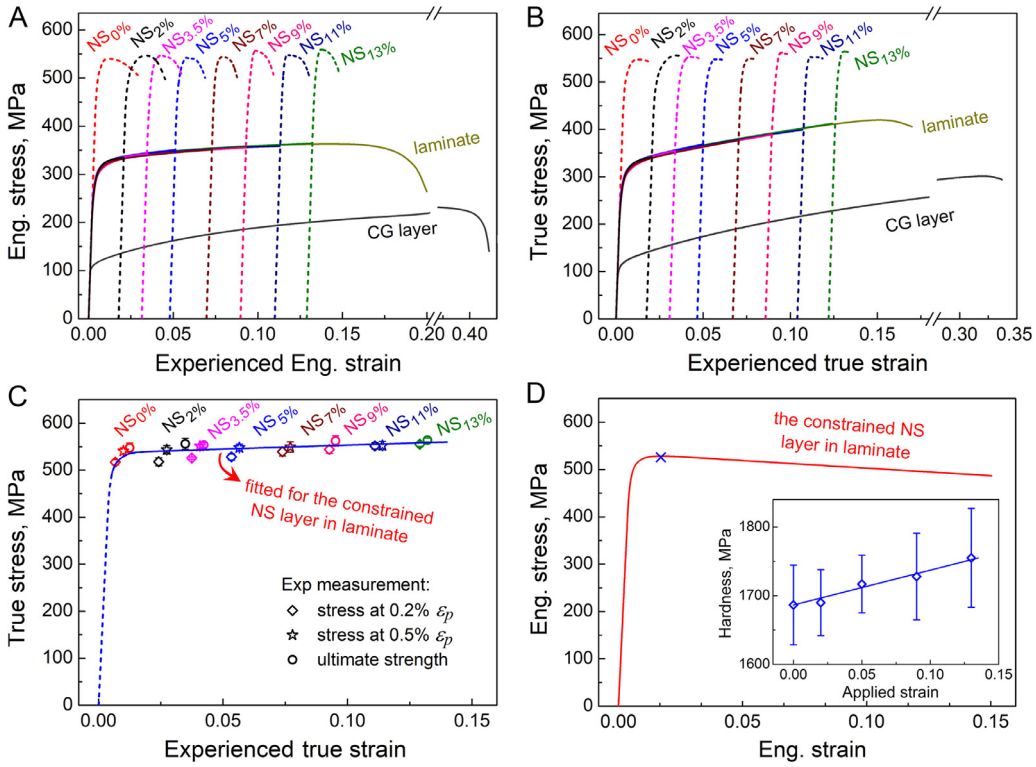

Fig. 2. Mechanical behavior of the constrained NS layer in laminate. (*A*) The engineering stress-strain curves of integrated laminate, freestanding CG layer and $NS_{x\%}$ specimens (the dotted curves). (*B*) The true stress-strain curves. The colored solid lines represent the prestraining process of laminate. (*C*) A fitted true stress-strain response of the constrained NS layer in laminate. (*D*) The engineering stress-strain response derived from the fitted curve in (*C*). The blue symbol × indicates the critical strain with maximum engineering strength. The insert in (*D*) shows the hardness evolution of the constrained NS layer, in which the error bar represents the standard deviation of 25 independent indentations.

Considering a situation like this: during the prestraining of laminate, a necking with serious shrinking in specimen width direction is formed at the critical strain of *y*%. The $NS_{x\%}$ specimen must exhibit lower tensile strength than the $NS_{y\%}$ specimen if *x*%>*y*%, because the necking zone has lower load-carrying capability as determined by Eq. (1). This logic indicates that as long as the strength of $NS_{x\%}$ specimen keeps increasing with the increase of prestrain, the deformation of the NS layer in laminate is still uniform at *x*% strain. Therefore, the uniform elongation of the NS layer in laminate should be the strain limit at which the fitted flow strength in Fig. 2*C* starts to decrease. As shown, it is larger than 13.5%.

The uniform deformation makes it reasonable to derive the engineering stress-strain response based on $\varepsilon_e = e^{\varepsilon_t} - 1$ and $\sigma_e = \sigma_t/(1+\varepsilon_e)$. As plotted in Fig. 2*D*, the uniform elongation of NS layer in laminate is accompanied by a continuous drop in engineering stress, i.e., gradual decrease of the carrying capability of total load. Interestingly, such behavior has never been observed in freestanding homogeneous material. For instance, in the tensile deformation of homogeneous NS and/or CG, $d\sigma_t A_t \geq -\sigma_t dA_t$ is a prerequisite for maintaining strain uniformity, which results in increased engineering stress [29]. This is the third mechanical peculiarity of constrained NS layer.

The comparison in Fig. 3 shows that the constrained NS layer in laminate achieves a superior combination of strength and uniform elongation, which is not accessible for a freestanding counterpart with homogeneous microstructure [32–39]. For example, with comparable strength above 500 MPa, the uniform elongation is 3-10 times larger than that of the freestanding NS material. This suggests that extra constraint enables the NS layer to get free from the trade-off curse of strength and uniform elongation [1,2,4].

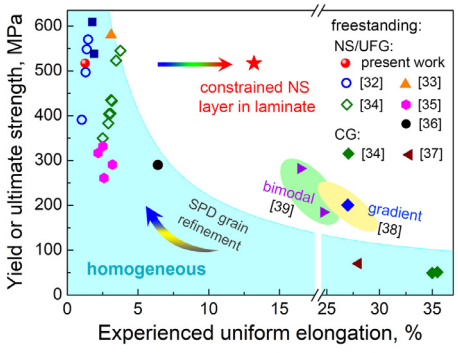

Fig. 3. The combination of strength and uniform elongation of the constrained NS layer in laminate, in comparison with the freestanding brasses (with 4.6-11wt.%Zn) characterized by conventional homogeneous microstructure or newly designed heterogeneous microstructure. The data of yield strength and ultimate strength are presented by solid and open symbols, respectively.

Microscopic strain distribution in the NS layer of laminate was mapped using in-situ μ-DIC technique (Figs. 4*A* and *B*) [8]. Dense micro strain bands are dispersed in the NS layer, as partially marked by black arrows in Fig. 4*B*. They intersect with each other and collectively accommodate large applied strain, but none of them developed unstably to fail the sample, resulting in globally homogeneous strain distribution. In other words, these strain bands are plastically stable. Fig. 4*C* shows the morphology of fully developed strain bands near fracture zone. Note that, in the uniform gauge section, no cracks appeared in strain bands, due to the limited strain concentration (< 30%). These observations suggest that the large uniform elongation of NS layer in laminate is accommodated by forming dense and dispersed stable micro strain bands.

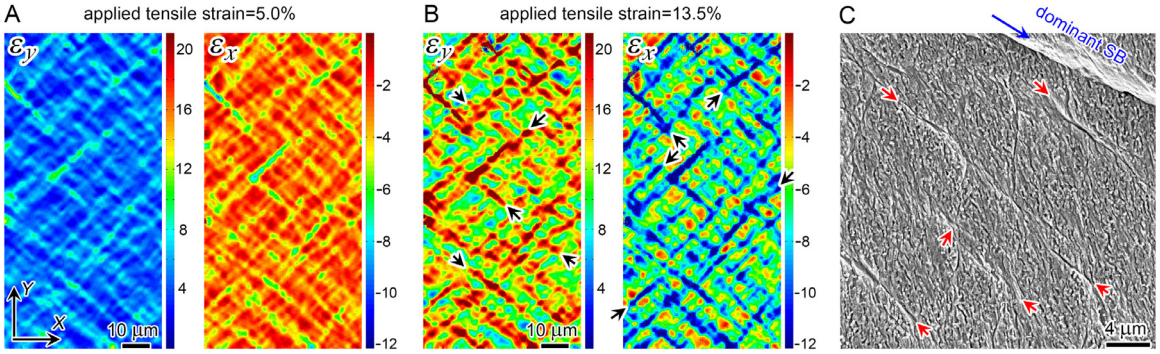

Fig. 4. Strain contours measured on the NS layer in laminate, at the applied tensile strain of (*A*) 5.0% and (*B*) 13.5%. The coordinate is same to that in Fig. 1. Strain bands are the strain concentration bands orientated at ~48° with respect to the tensile axis (warm-colored in ε_y contour and cold-colored in ε_x contour). (C) A SEM image showing the developed strain bands near fracture. Actually, due to the lack of long slip traces as that appeared in CG deformation, it's difficult to distinguish the strain bands in uniform gauge section directly from surface morphology, even if the surface is well-polished. Therefore, strain bands near fracture are presented here to show their morphology.

The nucleation of strain bands is primarily caused by insufficient strain hardening capability. Specifically, the work hardening of NS layer is not high enough to offset the geometrical softening, which renders an unstable state under mechanical perturbation, i.e., $dF = d\sigma_t A_t + \sigma_t dA_t < 0$ (Eq. (1)) [30,31]. Micro instability, i.e., strain bands nucleation, can be readily activated from the sites with higher distortion energy to relieve local stress concentration and accommodate strain [9,11]. However, when the micro strain bands propagate to meet the neighboring CG layer, the stress concentration at tip can be effectively reduced by the frequent dislocation slips, thereby being passivated or even suspended [23,24]. Moreover, the intersection of strain bands plays a role in preventing them from catastrophic propagation as well. The arrested early strain bands cannot relieve the stress concentration far away from them, which provides opportunity to nucleate more strain bands in virginal regions until they are dispersed over the whole NS layer [40]. In contrast, individual early strain band would propagate preferentially to dominate fracture and eliminate the opportunity of more strain bands nucleation, if there is no CG neighbor [28]. In other words, the constraint from CG layer played the key role in stabilizing strain bands and inducing dispersed nucleation.

This observation is consistent with the assertion that dispersed strain bands may be intrinsic to the deformation of heterostructure composed of NS and ductile zones, although the size and intensity of strain bands vary with the dimension and arrangement of zones [9,23,24,40].

Compared to the as-annealed microstructure (Fig 5*A*), the NS layer has obviously higher density of deformation nanotwins after tensile deformation (Fig. 5*B*). Nanotwins originated from grain boundary, with another end terminated in grain interior or at the opposite grain boundary (Fig. 5*C*). Such features provide evidence for the formation mechanism of Shockley partial emission from grain boundary [41,42]. As shown by the high resolution atomic-scale images, some nanotwins have clean boundary with matrix (Fig. 5*D*), whereas the boundary of others is decorated by thick stacking faults layer (Fig. 5*E*). These may indicate different twinning routes operated by varying partial behaviors [26,41]. Stacking fault clusters and ribbons are frequently observed as well (Fig. 5*F*). These results suggest that the crystallographic deformation of NS

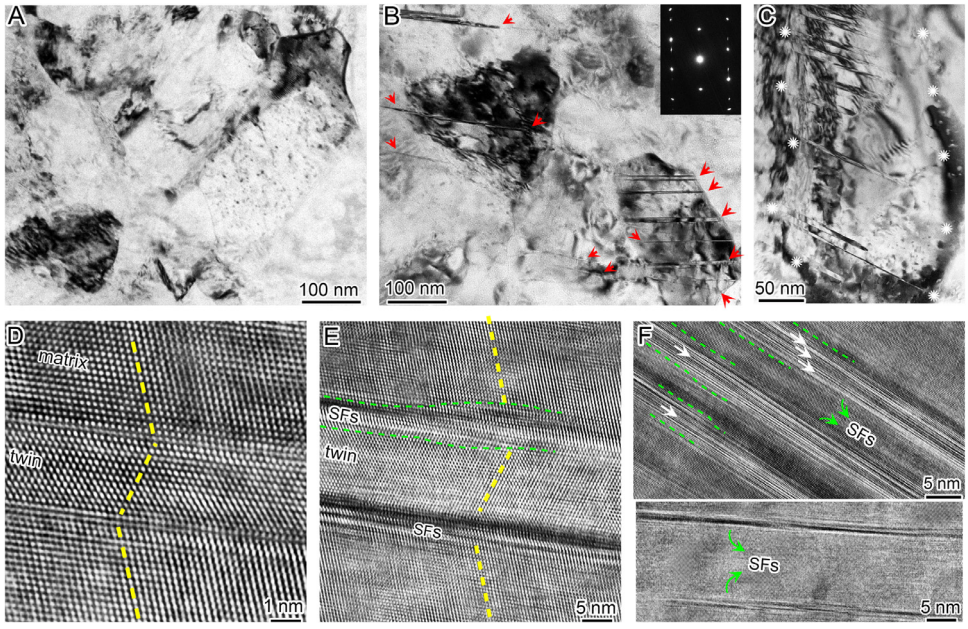

Fig. 5. TEM images of the constrained NS layer (*A*) before and (*B-F*) after tensile deformation. (*C*) An elongated grain, in which the white dots indicate grain boundary. (*D-F*) High resolution images taken from the grain shown in (*C*), showing the deformation twins and stacking faults (SFs). The red arrows in (*B*) indicate the nanotwins. The green lines in (*E*) and (*F*) mark the regions with high-density SFs.

layer in laminate is dominated by mechanical twinning and stacking faults.

For the NS brass with low stacking fault energy (35 mJ/m^2), the pre-existing defects enhances the strength, which promotes the emission of Shockley partials at higher stress, thereby facilitating twinning and stacking faults formation [42,43]. The twins and stacking faults act as both obstacles to dislocation motion and pathway for their glide, which leads to more dislocation accumulation and thus improves work hardening [26,41,43]. These physics are primarily responsible for the moderate strain hardening behavior of NS layer in laminate (Fig. 2).

Meanwhile, the work hardening also has favored effect on stabilizing strain bands and suppressing local cracking [44]. Note that these crystallographic mechanisms should be activated in both the strain banding and non-strain banding zones, and more frequently in the former due to the higher accumulative strain (Fig. 4). However, there is no opportunity for them to prevail homogeneously in a freestanding NS layer, due to the stress relief caused by quick strain localization.

In summary, in the tensile deformation of a NS/CG laminate, stress-strain response performed by the NS layer is quantitatively examined by a well-designed prestraning-peeling-retesting procedure. The work hardening afforded by mechanical twinning and stacking faults is weaker than geometrical softening, but constraint from the CG layers changes the strain path from quick catastrophic strain localization to the development of dense and dispersed stable micro strain bands. As a result, it displays a uniform elongation as large as 13.5%, moderate work hardening but gradually reduced engineering flow stress. The combination of strength and uniform elongation of the constrained NS layer is unattainable by freestanding homogeneous structure. These findings point out the mechanical advances of heterostructure design: combining the intrinsic superiority of multiple zones, and enabling extra improvement of zones' performance.

Declaration of Competing Interest

The authors declare that they have no conflict of interest.

Acknowledgments

This work was supported by the NSFC programs (Nos. 51931003, 11890681, 12032001 & 1210020469), the Postdoctoral Science Foundation of China (Nos. BX2021011 & 2020M680223), the National Key R&D Program of China (2017YFA0204403).

References

[1] Y.T. Zhu, K. Ameyama, P.M. Anderson, I.J. Beyerlein, H.J. Gao, H.S. Kim, E. Lavernia, S. Mathaudhu, H. Mughrabi, R.O. Ritchie, N. Tsuji, X.Y. Zhang, X.L. Wu, Mater. Res. Lett. 9 (2021) 1–31.
[2] X.L. Wu, Y.T. Zhu, Mater. Res. Lett. 5 (2017) 527–532.
[3] X.Y. Li, L. Lu, J.G. Li, X. Zhang, H.J. Gao, Nat. Rev. Mater. 5 (2020) 706–723.
[4] J.G. Li, Q. Zhang, R.R. Huang, X.Y. Li, H.J. Gao, Scr. Mater. 186 (2020) 304–311.
[5] T.H. Fang, W.L. Li, N.R. Tao, K. Lu, Science 331 (2011) 1587–1590.
[6] Z. Cheng, H.F. Zhou, Q.H. Lu, H.J. Gao, L. Lu, Science 362 (2018) eaau1925.
[7] X.L. Wu, P. Jiang, L. Chen, F.P. Yuan, Y.T. Zhu, Proc. Natl. Acad. Sci. U.S.A. 111 (2014) 7197–7201.
[8] C.X. Huang, Y.F. Wang, X.L. Ma, S. Yin, H.W. Höppel, M. Göken, X.L. Wu, H.J. Gao, Y.T. Zhu, Mater. Today 21 (2018) 713–719.
[9] M. Huang, C. Xu, G.H. Fan, E. Maawad, W.M. Gan, L. Geng, F.X. Lin, G.Z. Tang, H. Wu, Y. Du, D.Y. Li, K.S. Miao, T.T. Zhang, X.S. Yang, Y.P. Xia, G.J. Cao, H.J. Kang, T.M. Wang, T.Q. Xiao, H.L. Xie, Acta Mater 153 (2018) 235–249.
[10] X.L. Wu, M.X. Yang, F.P. Yuan, G.L. Wu, Y.J. Wei, X.X. Huang, Y.T. Zhu, Proc. Natl. Acad. Sci. U.S.A. 112 (2015) 14501–14505.
[11] P. Sathiyamoorthi, H.S. Kim, Prog. Mater. Sci. (2020) 100709.
[12] X.L. Wu, M.X. Yang, R.G. Li, P. Jiang, F.P. Yuan, Y.D. Wang, Y.T. Zhu, Y.G. Wei, Sci. China Mater. 64 (2021) 1534–1544.
[13] Y.F. Wang, C.X. Huang, Z.K. Li, X.T. Fang, M.S. Wang, Q. He, F.J. Guo, Y.T. Zhu, Extreme Mech. Lett. 37 (2020) 100686.
[14] T. Wan, Z. Cheng, L.F. Bu, L. Lu, Scr. Mater. 201 (2021) 113975.
[15] Z. Zeng, X.Y. Li, D.S. Xu, L. Lu, H.J. Gao, T. Zhu, Extreme Mech. Lett. 8 (2016) 213–219.
[16] Y.F. Wang, M.X. Yang, X.L. Ma, M.S. Wang, K. Yin, A.H. Huang, C.X. Huang, Mater. Sci. Eng. A 727 (2018) 113–118.
[17] Y.F. Wang, M.S. Wang, X.T. Fang, F.J. Guo, H.Q. Liu, R.O. Scattergood, C.X. Huang, Y.T. Zhu, Int. J. Plast. 123 (2019) 196–207.
[18] H.K. Park, K. Ameyama, J. Yoo, H. Hwang, H.S. Kim, Mater. Res. Lett. 6 (2018) 261–267.
[19] Y.F. Wang, Y.T. Zhu, X.L. Wu, Y.G. Wei, C.X. Huang, Sci. China Mater. (2021), doi:10.1007/s40843-021-1702-2.
[20] M.F. Ashby, Philos. Mag. 21 (1970) 399–424.
[21] Y.T. Zhu, X.L. Wu, Mater. Res. Lett. 7 (2019) 393–398.
[22] Y.F. Wang, C.X. Huang, X.T. Fang, H.W. Höppel, M. Göken, Y.T. Zhu, Scr. Mater. 174 (2020) 19–23.
[23] Y.F. Wang, C.X. Huang, Y.S. Li, F.J. Guo, Q. He, M.S. Wang, X.L. Wu, R.O. Scattergood, Y.T. Zhu, Int. J. Plast. 124 (2020) 186–198.
[24] Y.F. Wang, C.X. Huang, Q. He, F.J. Guo, M.S. Wang, L.Y. Song, Y.T. Zhu, Scr. Mater. 170 (2019) 76–80.
[25] K. Lu, Science 345 (2014) 1455–1456.
[26] P.J. Shi, Y.B. Zhong, Y. Li, W.L. Ren, T.X. Zheng, Z. Shen, B. Yang, J.C. Peng, P.F. Hu, Y. Zhang, P.K. Liaw, Y.T. Zhu, Mater. Today 41 (2020) 62–71.
[27] M.X. Yang, Y. Pan, F.P. Yuan, Y.T. Zhu, X.L. Wu, Mater. Res. Lett. 4 (2016) 145–151.
[28] I.A. Ovid'ko, R.Z. Valiev, Y.T. Zhu, Prog. Mater. Sci. 94 (2018) 462–540.
[29] Y.T. Zhu, X.L. Wu, Mater. Today Nano 2 (2018) 15–20.
[30] T. Li, Z. Suo, Int. J. Solid. Struct. 43 (2006) 2351–2363.
[31] T. Li, Z. Suo, Int. J. Solid. Struct. 44 (2007) 1696–1705.
[32] P. Zhang, S. Qu, M.X. Yang, G. Yang, S.D. Wu, S.X. Li, Z.F. Zhang, Mater. Sci. Eng. A 594 (2014) 309–320.
[33] Y.H. Zhao, Y.T. Zhu, X.Z. Liao, Z. Horita, T.G. Langdon, Appl. Physic. Lett. 89 (2006) 121906.
[34] Z.J. Zhang, Q.Q. Duan, X.H. An, S.D. Wu, G. Yang, Z.F. Zhang, Mater. Sci. Eng. A 528 (2011) 4259–4267.
[35] P.C. Yadav, A. Sinhal, S. Sahu, A. Roy, S. Shekhar, J. Mater. Eng. Perform. 25 (2016) 2604–2614.
[36] P.C. Yadav, N.K. Sharma, S. Sahu, S. Shekhar, Materials Chemistry and Physics 238 (2019) 121912.
[37] S.M. Dasharath, S. Mula, Mater. Sci. Eng. A 675 (2016) 403–414.
[38] B.Z. Cai, X.L. Ma, J. Moering, H. Zhou, X.C. Yang, X.K. Zhu, Mater. Sci. Eng. A 626 (2015) 144–149.
[39] V. Subramanya, K. Sivaprasad, D. Sturm, M. Heilmaier, Materials Science and Engineering: A 489 (2008) 253–258.
[40] G. He, J. Eckert, W. Löser, L. Schultz, Nat. Mater. 2 (2003) 33–37.
[41] Y.T. Zhu, X.Z. Liao, X.L. Wu, Prog. Mater. Sci. 57 (2012) 1–62.
[42] Y.T. Zhu, X.L. Wu, X.Z. Liao, J. Narayan, S.N. Mathaudhu, L.J. Kecskés, Appl. Phys. Lett. 95 (2009) 031909.
[43] Z.W. Wang, Y.B. Wang, X.Z. Liao, Y.H. Zhao, E.J. Lavernia, Y.T. Zhu, Z. Horita, T.G. Langdon, Scr. Mater. 60 (2009) 52–55.
[44] F.P. Yuan, D.S. Yan, J.D. Sun, L.L. Zhou, Y.T. Zhu, X.L. Wu, Mater. Res. Lett. 7 (2019) 12–17.